JMEPEG (2012) 21:1070–1075
DOI: 10.1007/s11665-011-9978-0

1059-9495/$19.00

Effects of Severe Cold Rolling on Exfoliation Corrosion Behavior of Al-Zn-Mg-Cu-Cr Alloy

Lianghua Lin, Zhiyi Liu, Yao Li, Xiangnan Han, and Xu Chen

(Submitted October 8, 2010; in revised form April 11, 2011)

The exfoliation corrosion (EXCO) behavior of Al-Zn-Mg-Cu-Cr alloy after severe cold rolling was investigated by optical microscope, transmission electron microscope, and electrochemical technique. The results show that the EXCO resistance decreased with increasing cold rolling reduction because of the grain boundaries which were decorated with the continuously distributed particles. After the solution treatment, the samples with different reductions retained the fibrous grains, and the elongated grains accelerated the growth of the corrosion cracks according to crack propagation analysis. Furthermore, the increase of deformation enhanced the degree of recrystallization, while the number of corrosion cells increased greatly when in the electrolyte, which tended to reduce the resistance to EXCO.

Keywords crack propagation, exfoliation corrosion, recrystallization, severe cold rolling

1. Introduction

Exfoliation corrosion (EXCO) is a particular form of intergranular corrosion that tends to associate with aluminum alloys that have been rolled or extruded, with an elongated grain structure (Ref 1). Alloys of 2XXX and 7XXX, which contain zinc or magnesium as alloying constituents, are the most prone to this type of corrosion. In this particular form of intergranular corrosion, the expansive force of insoluble corrosion products tends to force the grains apart and promote further attack, which leads to various types of material degradation ranging from pitting or flaking to the formation of large blisters (Ref 2). Owing to loss in mechanical properties of Al alloys, EXCO is a significant source of life-limiting degradation in airframes (Ref 3).

The main reason for EXCO can be attributed to the galvanic interaction between the grain boundary precipitates and the adjacent matrix. Thus, the heat-treatment conditions of the alloy are thought to be key factors in exfoliation (Ref 4). It has been reported that artificial aging to the T7 or RRA (Retrogression and re-aging) temper provides improved resistance by changing the size and particle interval of the grain boundary precipitates (Ref 5, 6). Microalloying elements also play a significant role, for example, the chromium-and-manganese-containing alloy exhibits generally a much worse exfoliation behavior than the chromium and manganese-free alloy (Ref 2, 7). Fang et al. (Ref 8) found the additions of Zr and Yb in Al-Zn-Mg-Cu alloy facilitated the formation of low angle grain boundaries (LAGB), and subsequently remarkably enhanced the resistance to EXCO. Maitra and English (Ref 4) had attributed the corrosion susceptibility of AA7075-T6 to Mg and Zn solute segregation or enrichment in the grain boundary region, and so the Zn/Mg ratio can be an important factor in EXCO.

Although the influence of the heat treatment of different compositions of Al-Zn-Mg-Cu alloy is well documented, no study has as yet been devoted to the understanding of the severe cold rolling affecting the EXCO behavior. It is well known that the microstructure of metal changes in several ways during deformation. First, and most obvious, the grains change their shape, and there is a surprisingly large increase in the total grain boundary area (Ref 9). A second obvious feature is the accumulation of dislocations. The sum of the energies of all the dislocations and new interfaces represents the stored energy deformation, which provides the driving force for recovery and recrystallization. There is the possibility that the changes mentioned above might affect the EXCO susceptibility of Al-Zn-Mg-Cu alloy. Therefore, this study aims to investigate the effect of severe cold rolling on grain aspect ratio and the resultant susceptibility to EXCO in an Al-Zn-Mg-Cu aluminum alloy.

2. Experimental Procedures

The Al-Zn-Mg-Cu-Cr alloy casting was used as the raw material and the chemical composition of the alloys were 6.11 wt.% Zn, 2.76 wt.% Mg, 1.91 wt.% Cu, 0.25 wt.% Cr, 0.04Ti, and balance Al. Plates of 20-mm thickness plates were cut from the casting and were homogenized at 470 °C for 24 h, and then quenched. The homogenized plates were hot rolled to a thickness of 6 mm at 390 °C, annealed at 410 °C, and cold rolled at ambient temperature to plates of 3 mm (sample CR5), 2.5 mm (sample CR6), 2 mm (sample CR7), and 1.5 mm (sample CR8) thickness (the cold rolled reductions are 50, 60, 70, and 80%, respectively). All of the samples were solution treated for 1 h at 470 °C and cold water quenched, and then aged for 3 h at 125 °C plus 10 h at 170 °C.

Lianghua Lin and **Zhiyi Liu**, Key Laboratory of Nonferrous Metal Materials Science and Engineering, Ministry of Education, Central South University, Changsha 410083, People's Republic of China; and **Lianghua Lin, Zhiyi Liu, Yao Li, Xiangnan Han,** and **Xu Chen**, School of Material Science and Engineering, Central South University, Changsha 410083, People's Republic of China. Contact e-mail: liuzhiyi@mail.csu.edu.cn.

The accelerated EXCO tests were carried out at room temperature according to EXCO test of ASTM Standard (Ref 10) G34-90. Samples of 100 mm × 30 mm were prepared from the cold rolled sheet the long axis of the rectangle of which was parallel to the rolled direction. The EXCO solution consisted of 4.0 M NaCl + 0.5 M KNO_3 + 0.1 M HNO_3 diluted to 1 L with distilled water. Before the test, the samples were degreased by ultrasonicating in propanone, and the non-test surfaces were masked using epoxide resin. After the pretreatment, the samples were immersed in the EXCO solution. The solution in sufficient quantity is utilized to provide a volume-to-metal surface area ratio of 15 mL cm^{-2}. After 48 h of continuous immersion in the solution, the morphologies of the alloys were recorded, and the depths of attack were measured under the optical microscope.

Potentiodynamic polarization curves were carried out using the Solartron 1287 electrochemical system. A saturated calomel electrode was used as the reference electrode, a platinum electrode as the auxiliary electrode, and 1 cm^2 of the alloy being studied as the working electrode; the test solution was prepared in the same way as the EXCO testing solution, and the solution temperature was maintained at 25 °C.

Microstructures were observed using an optical microscope for solution-treated specimens which were polished and etched in Keller's reagent. The specimens were also investigated by transmission electron microscope (TEM), the thin foils were prepared by double-jet electropolishing at 20 V in a solution of 30% nitric acid, and 70% methanol solution cooled to −25 °C, and observed in a Tecnai$G^2$20 TEM operated at 200 kV.

3. Results and Discussion

Figure 1 presents photographs of Al-Zn-Mg-Cu-Cr alloy samples cold rolled to 50, 60, 70, and 80% thickness reductions after immersing in the test solution for 48 h. It shows that, the CR5 sample exhibited a slight exfoliation attack, where only few zones showed a dark gray appearance because of corrosion products. On the sheet surface, both tiny pits and light lifting of metal at the pit edges can be seen. However, the original metallic surface was mostly visible. With increasing reduction, the CR6 or CR7 samples with obvious lifted surface layers had worse appearance than the CR5 sample. When the reduction was up to 80%, the surface of CR8 sample bulged outward severely. It is clear that the sample's resistance to EXCO was remarkably reduced as the cold-rolling reduction increased. EXCO rating can be summarized as EA, EA+, EB, and EB+, according to ASTM standard evaluation criteria.

There appears to be a close relationship between stress corrosion cracking and exfoliation in high strength aluminum alloy, as both of them forms intergranular corrosion and both require a tensile component of stress at the developing corrosion tip. If the edge layer is still present after the test, then this would help us identify the EXCO rating from the estimate of the depth of corrosion attack. Figure 2 shows the maximum depth of attack on Al-Zn-Mg-Cu-Cr alloy in the EXCO test for 48 h. The maximum depth of attack on CR5 sample was 172 μm (Fig. 2a), while the maximum depth of attack on CR8 sample was up to 376 μm (Fig. 2d).This further indicated that severe cold rolled reductions promoted exfoliation. Figure 2 also shows how exfoliation is developed by corrosion along boundaries of the elongated grains. As corrosion proceeded along multiple narrow paths parallel to the roll-direction, the insoluble products occupied a larger volume than the metal, which then produced wedging stresses, resulting in the flaking and delamination of uncorroded layers of metal.

The potentiodynamic polarization curves for different rolled samples in EXCO solution are illustrated in Fig. 3. In order to measure the corrosion potential (E_{corr}) as well as the corrosion current density (I_{corr}), Tafel's extrapolation method based on electrochemical polarization was employed. Electrochemical characteristics derived from the polarization curves are summarized in Table 1. As shown in the table, the value of corrosion potential was the most negative for CR8 sample, but the most positive for CR5 sample. Further, the E_{corr} shifted

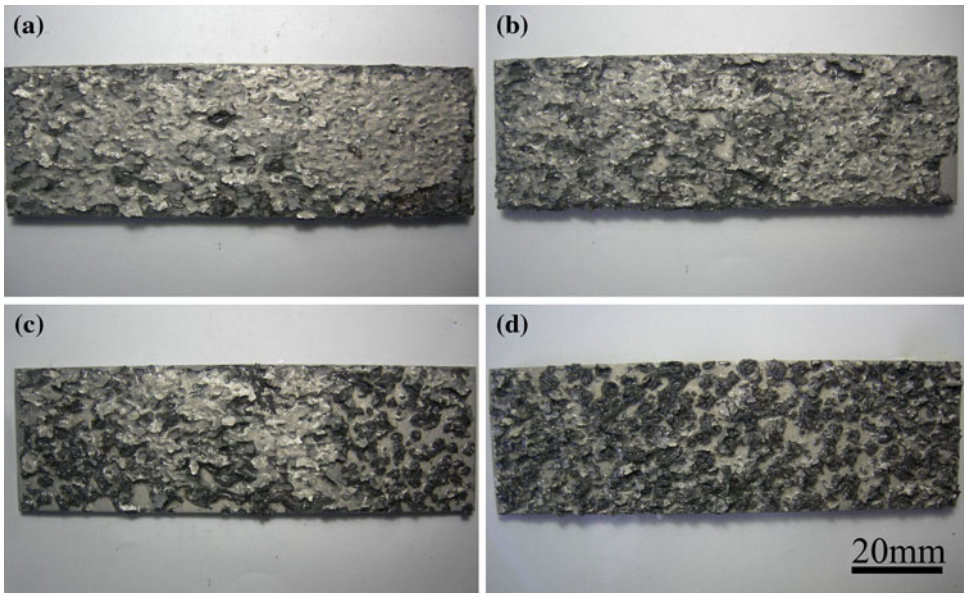

Fig. 1 Photographs of Al-Zn-Mg-Cu-Cr alloy of various cold rolled reduction after 48 h of exfoliation test: (a) CR5, (b) CR6, (c) CR7, and (d) CR8 samples

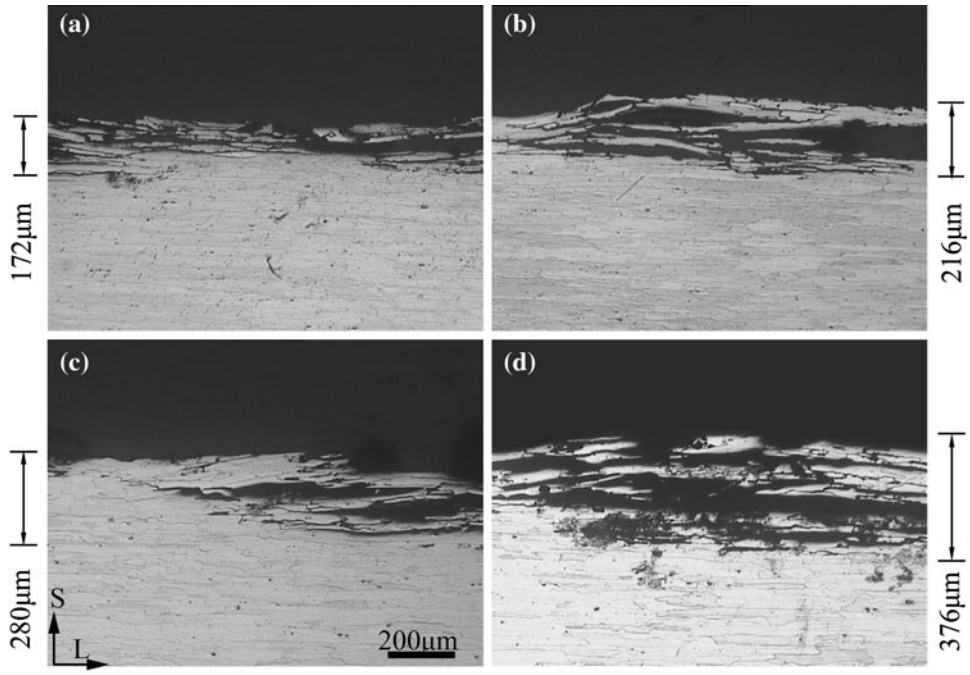

Fig. 2 Cross-sectional micrographs of (a) CR5, (b) CR6, (c) CR7, and (d) CR8 samples exposed to exfoliation solution for 48 h; the maximum depths of attack are 172, 216, 280, and 376 μm, respectively

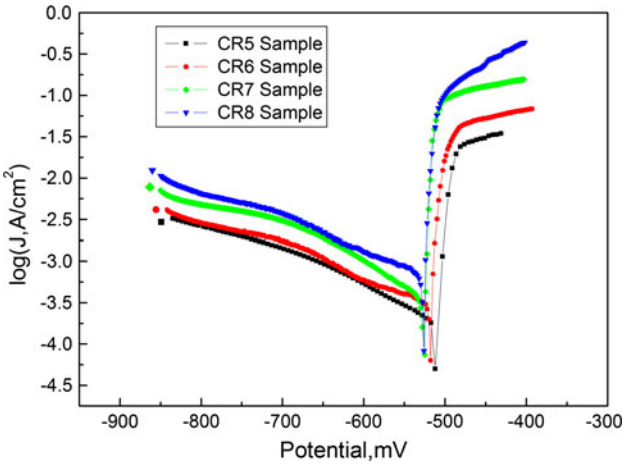

Fig. 3 Polarization curves of Al-Zn-Mg-Cu-Cr alloy in EXCO solution at the scan rate of 0.2 mV s^{-1}

from −526 mV in CR8 sample to −512 mV in CR5 sample, and the I_{corr} decreased from 602 to 187 μA cm^{-2}, respectively. These results suggested that the corrosion susceptibility increases with increasing the cold-rolling reductions, according to Faraday's law which states that the electrochemical corrosion rate increases linearly with the corrosion current density I_{corr}. This indicates a good correlation between the results from immersion testing: the depth of corrosion attack measurement and potentiodynamic polarization measurement.

It is widely accepted that the rate of EXCO is directly related to the grain boundary precipitates (Ref 11). Figure 4 illustrates the grain boundary precipitates of Al-Zn-Mg-Cu-Cr alloys with various rolled reductions. The CR5 and CR6 samples showed some discontinuity in the arrangement of precipitates along the grain boundary. With increasing cold rolling reduction, the

Table 1 Summary of corrosion parameters obtained from the polarization curves

Sample	Rolling reduction, %	E_{corr}, mV	I_{corr}, μA cm^{-2}
CR5	50	−512	187
CR6	60	−518	317
CR7	70	−525	391
CR8	80	−526	602

interval of the grain boundary precipitates decreased, while the CR8 sample of 80% deformation showed the continuous presence of precipitates along the grain boundary. As well as we have known, the main precipitations which dominate hardening in Al-Zn-Mg-Cu alloys are the η′ phase and η phases after a two-stage process (Ref 12). In comparison with the former, the activation energy for nucleation of stable η phase is much higher. In order to lower the total free energy, nuclei of η phase form preferentially at dislocations and grain boundaries. While the amount of deformations had been increased before artificial aging, the density of dislocations became higher, especially in grain boundaries, which is attributed to the continuous presence of precipitates along the grain boundary (Ref 13), as can be seen in Fig. 4(a)-(d).

In general, the precipitates on the grain boundaries (mainly of Zn-rich phases) have the electrode potential different from that of the aluminum matrix, which is anodic to the aluminum matrix and is preferentially attacked in chloride solution. Consequently, the corrosion product generates large wedging stresses that lift the surface grains. In Fig. 1 and 2, the CR8 sample was more susceptible to EXCO than other samples. This can be attributed to the continuous precipitates in grain boundaries (Fig. 4d), which produced an ionic-conducting path between the anode and cathode, by which chlorides solution

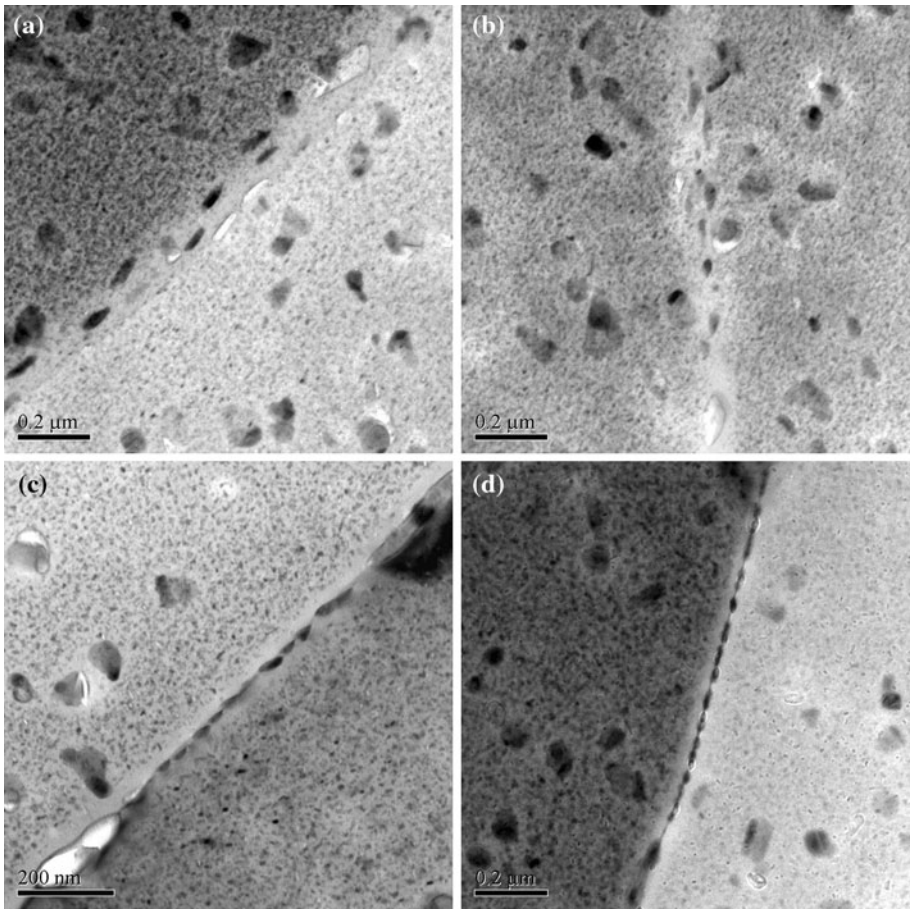

Fig. 4 TEM micrographs showing grain boundary precipitates of Al-Zn-Mg-Cu-Cr alloys with various rolled reductions: (a) CR5, (b) CR6, (c) CR7, and (d) CR8 samples

can reach crack tips, and the corrosion rate can proceed more rapidly. On the contrary, the alloys with discontinuous precipitates in grain boundaries possess a better EXCO resistance. Furthermore, the result can also be explained in terms of the theory of hydrogen embrittlement. Such a theory implies that there may exist Mg-H complexes leading to grain embrittlement in the process of corrosion (Ref 14). In Al-Zn-Mg-Cu-Cr alloy, the affinity of the Mg and H atoms is larger than that of Al and H atoms in terms of the electronegativity difference. Therefore, Mg segregation at grain boundary enhances the amount of hydrogen absorbed and increased the solution of hydrogen, resulting in hydrogen embrittlement and leading to further grain boundary embrittlement (Ref 15). However, the increase in the size and interparticle spacing of the grain boundary precipitates acted as the trapping sites for atomic hydrogen and created molecular hydrogen bubbles, which would reduce the concentration of the atomic hydrogen on the grain boundaries, thus explaining why the EXCO resistance decreased as the rolling reduction increased.

In addition, many studies have shown that the grain size and shape could be also an important factor in EXCO (Ref 16-18). Figure 5 presents optical micrograph of Al-Zn-Mg-Cu-Cr sheets after solution treatment. All the as-rolled specimens were partially recrystallized after annealing at 470 °C for 1 h, and the grain boundaries remained aligned to the rolling direction. This elongated grain may be explained with the traces of chromium existing in Al-Zn-Mg-Cu-Cr alloy. The addition Cr to Al-Zn-Mg-Cu alloy can remarkably inhibit the recrystallization during solution heat treatment, while the presence of Cr-containing dispersoids can stabilize. the deformation microstructure by pinning the subgrain boundaries (Ref 19). In Fig. 5, the grain width for CR5 sample ranged from 50 to 70 μm, while the 80% rolled CR8 sample ranged from 10 to 30 μm. Clearly, the thickness reduction of cold rolling greatly contributed to the increasing of the grain aspect ratios of Al-Zn-Mg-Cu-Cr cold rolled sheets after solution treatment. On the other hand, as the rolling reduction was increased, the volume of recrystallization grains increased with the simultaneous increase in the total grain boundary area after solution treatment. Therefore, the number of corrosive cells consisting of grain boundary and aluminum matrix enhanced greatly when remaining in electrolyte. Consequently, the CR8 sample exhibits the highest corrosion current density I_{corr} value as shown in Table 1.

A schematic representation of the growth of cracks in exfoliation alloys in two dimensions is given in Fig. 6, showing the situation that the crack tip has arrived at a triple point of the grain boundary at the top. In the figure, the homogeneous trajectory is the direction the crack would propagate in isotropic, θ_1 and θ_2 represent the angles between the homogeneous trajectory and the new crack path's direction, with the corresponding stresses being σ_1 and σ_2, respectively. Using the principles of fracture mechanics, the critical stress σ_c required for crack propagation is described by Ref 20.

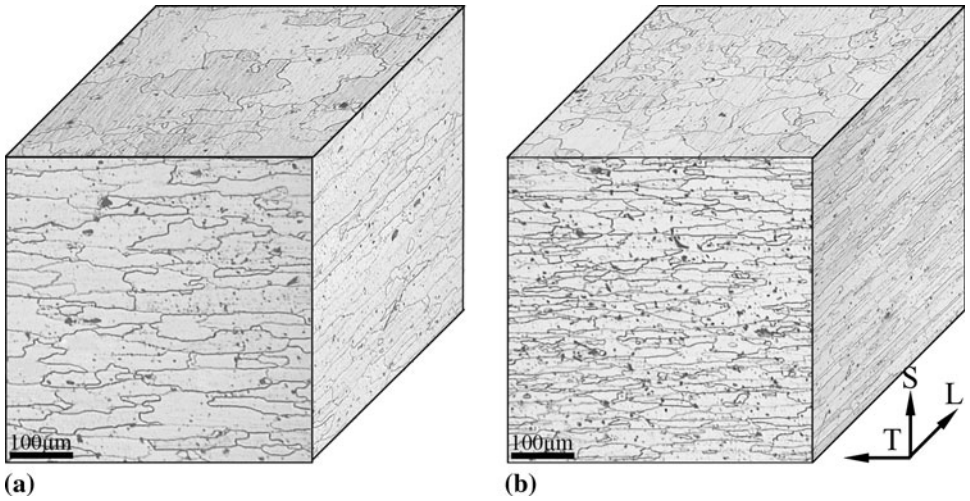

Fig. 5 Optical micrographs showing grain structures in cold rolled material after solution treatment: (a) CR5 and (b) CR8 samples

$$\sigma_c = \left(\frac{2E\gamma_s}{\pi a}\right)^{1/2} \quad \text{(Eq 1)}$$

where E is the modulus of elasticity, γ_s the specific surface energy, and a is one half the length of an internal crack. As previously analyzed, the corrosion cracks were generated by the stress that arises from the wedging effect of the voluminous corrosion products. When the stress produced by corrosion production exceeds the value of this critical stress, a crack forms and then propagates. The crack's velocity is predicted to have the form as suggested by Arkadi and Gerard (Ref 21):

$$V_C = c_R\left(1 - \frac{\Gamma}{G}\right) \quad \text{(Eq 2)}$$

where Γ is the specific fracture energy, c_R is the Rayleigh wave speed, and G is the amount of energy per unit area present at the tip of a static crack. As the cracks grow fast over the first grain facet, but slowly over the grain-boundary junction, the overall crack growth rate is expected to be controlled by the latter condition. For a crack propagating, G is related to the stress intensity, K, at the crack tip (Ref 22).

$$G = K^2\left(\frac{1-\upsilon^2}{E}\right) \quad \text{(Eq 3)}$$

As the stress intensity $K = \sigma\sqrt{\pi a}$ then

$$G = \pi a\left(\frac{1-\upsilon^2}{E}\right)\sigma^2 \quad \text{(Eq 4)}$$

Substitution of Eq 4 into Eq 2 gives

$$V_C = c_R\left(1 - \frac{E\Gamma}{\pi a(1-\upsilon^2)\sigma^2}\right) \quad \text{(Eq 5)}$$

It can be seen from Eq 5 that the velocity is recorded as a function of the square of the stress (σ^2). In Fig. 6, it is clear that $\theta_2 < \theta_1$, as, $\sigma_1 = \sigma_0 \cos\theta_1$, $\sigma_2 = \sigma_0 \cos\theta_2$; therefore, $\sigma_1 < \sigma_2$. Thus, as the stress increases, the crack propagation rate rises. In other words, the angle θ can contribute to the resistance-to-crack growth by reducing the driving force at the crack tip. According to two-dimensional fracture mechanics estimation (Ref 23), the tilt crack deflection degrades the stress intensity factor at the crack tip, resulting in a decreasing driving force for the crack propagation. Another reason for the increased resistance is that the area on grain boundaries has to be fractured for the crack to pass through the grain boundary (Ref 24). In Fig. 6, it seems clear that the area of AOB is of course proportional to the angle θ, so that more resistance to crack growth will be offered by the grain boundaries with large value of θ. In practice, this means that more elongated grain shape produced a larger wedging stress along the grain boundary, which caused a bigger stress concentration at the tip of crack and resulted in higher crack propagation rate.

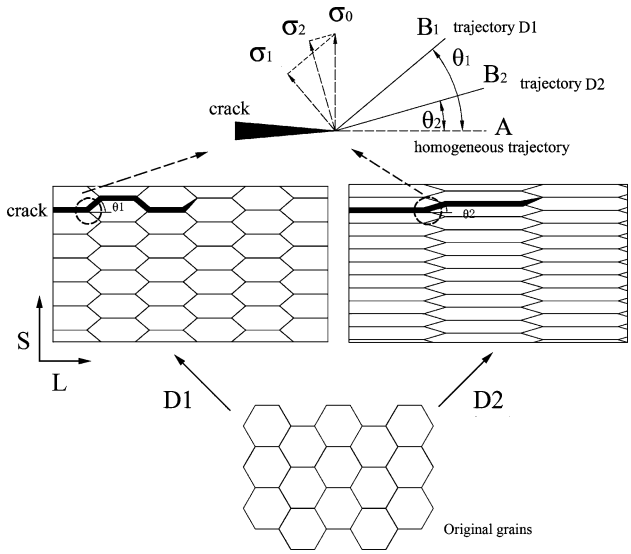

Fig. 6 Schematic representation of the crack propagations in Al-Zn-Mg-Cu-Cr alloys, D1, and D2 subjected to slight and severe cold rolling, respectively. θ represents the angle between the homogeneous trajectory and the new crack path's direction; the corresponding stress is σ; and the subscript 1 or 2 indicates the D1 or D2 deformation

4. Conclusions

On studying the effect of the degree of deformation on EXCO resistance of Al-Zn-Mg-Cu-Cr alloy, the following conclusions can be drawn:

1. Severe deformation caused continuous distribution of the η precipitates at the grain boundary. The EXCO resistance of Al-Zn-Mg-Cu-Cr alloy decreased with increasing cold-rolling reduction.
2. The grain shape of the material determined the length of corrosion path. More elongated grain shape produced a larger wedging stress along the grain boundary, resulting in a higher crack propagation rate.
3. The increase of deformation enhanced the degree of recrystallization, while the number of corrosive cells enhanced in EXCO solution, which tended to cause more rapid EXCO.

Acknowledgment

The authors would like to acknowledge the financial support provided by the National Key Fundamental Research Project of China (Grant No. 2005CB623705-04).

References

1. M.J. Robinson and N.C. Jackson, The Influence of Grain Structure and Intergranular Corrosion Rate on Exfoliation and Stress Corrosion Cracking of High Strength Al-Cu-Mg Alloy, *Corros. Sci.*, 1999, **41**(5), p 1013–1028
2. J. Wloka, T. Hack, and S. Virtanen, Influence of Temper and Surface Condition on the Exfoliation Behavior of High Strength Al-Zn-Mg-Cu Alloys, *Corros. Sci.*, 2007, **49**, p 1437–1449
3. J.P. Chubb and T.A. Morad, The Effect of Exfoliation Corrosion on the Fracture and Fatigue Behavior of 7178-T6 Aluminum, *Int. J. Fatigue*, 1995, **17**, p 49–54
4. S. Maitra and G.C. English, Mechanism of Localized Corrosion of 7050 Alloy Plate, *Metall. Trans.*, 1981, **12A**, p 535–541
5. J.C. Lin, H.L. Liao, and W.D. Jehng, Effect of Heat Treatments on the Tensile Strength and SCC-Resistance of AA7050 in an Alkaline Saline Solution, *Corros. Sci.*, 2006, **48**(10), p 3139–3456
6. F. Hamidreza, H. Babak, and Y. Mousa, The Effect of the Surface Treating and High-Temperature Aging on the Strength and SCC Susceptibility of 7075 Aluminum Alloy, *J. Mater. Eng. Perform.*, 2010, **19**(6), p 852–859
7. J.F. Li, N. Birbilis, and C.X. Li, Influence of Retrogression Temperature and Time on the Mechanical Properties and Exfoliation Corrosion Behavior of Aluminum AA7150, *Mater. Charact.*, 2009, **60**, p 1334–1341
8. H.C. Fang, K.H. Chen, and X. Chen, Effect of Cr, Yb and Zr Additions on Localized Corrosion of Al-Zn-Mg-Cu Alloy, *Corros. Sci.*, 2009, **51**, p 2872–2877
9. F.J. Humphreys and M. Hatherly, *Recrystallization and Related Annealing Phenomena*, Elsevier, London, 2004, p 11–15
10. ASTM Standard G34-90, *Standard Test Method for Ecorrosion Susceptibility in 2XXX and 7XXX Series Al Alloys*, 1990
11. D. Wang and Z.Y. Ma, Effect of Pre-Strain on Microstructure and Stress Corrosion Cracking of Over-Aged 7050 Aluminum Alloy, *J. Alloys Compd.*, 2009, **469**(1–2), p 445–450
12. K. Stiller, P.J. Warren, and V. Hansen, Investigation of Precipitation in an Al-Zn-Mg Alloy After Two-Step Ageing Treatment an 100 and 150 °C, *Mater. Sci. Eng. A*, 1999, **270**(1–2), p 55–63
13. G. Waterloo and V. Hansen, Effect of Pre-Deformation and Preaging at Room Temperature in Al-Zn-Mg-(Cu, Zr) Alloys, *Mater. Sci. Eng. A*, 2001, **303**(1–2), p 226–233
14. R.G. Song, M.K. Tseng, B.J. Zhang, J. Liu, Z.H. Jin, and K.S. Shin, Grain Boundary Segregation and Hydrogen-induced Fracture in 7050 Aluminum Alloy, *Acta Mater.*, 1996, **44**(8), p 3241–3248
15. R.G. Song, W. Dietzel, and B.J. Zhang, Stress Corrosion Cracking and Hydrogen Embrittlement of an Al-Zn-Mg-Cu Alloy, *Acta Mater.*, 2004, **52**(16), p 4727–4743
16. X.Y. Zhao and G.S. Frankel, Quantitative Study of Exfoliation Corrosion: Exfoliation of Slices in Humidity Technique, *Corros. Sci.*, 2007, **49**(2), p 920–938
17. M.J. Robinson and N.C. Jackson, Exfoliation Corrosion of High Strength Al-Cu-Mg Alloys: Effect of Grain Structure, *Br. Corros. J.*, 1999, **34**(1), p 45–49
18. M.J. Robinson and N.C. Jackson, The Influence of Grain Structure and Intergranular Corrosion Rate on Exfoliation and Stress Corrosion Cracking of High Strength Al-Cu-Mg Alloys, *Corros. Sci.*, 1999, **41**, p 1013–1028
19. K.H. Chen and H.C. Fang, Effect of Yb, Cr and Zr Additions on Recrystallization and Corrosion Resistance of Al-Zn-Mg-Cu Alloys, *Mater. Sci. Eng. A*, 2008, **497**(1–2), p 426–431
20. D. William and J. Callister, *Fundamentals of Materials Science and Engineering*, John Wiley, New York, 2001, p 238–248
21. B. Arkadi and A. Gerard, On the Propagation Velocity of a Straight Brittle Crack, *Int. J. Fract.*, 2007, **143**, p 135–142
22. L. Paul Hancock, *Continental Deformation*, Pergamon Press, Oxford, 1994
23. S. Suresh, Crack Deflection: Implications for the Growth of Long and Short Fatigue Cracks, *Metall. Trans. A*, 1983, **14A**, p 2375–2385
24. T. Zhai, A.J. Wilkinson, and J.W. Martin, A Crystallographic Mechanism for Fatigue Crack Propagation Through Grain Boundaries, *Acta Mater.*, 2000, **48**(20), p 4917–4927